Understanding luminescence properties of grain boundaries in GaN thin films and their atomistic origin

Hyobin Yoo, Sangmoon Yoon, Kunook Chung, Seoung-Hun Kang, Young-Kyun Kwon, Gyu-Chul Yi, and Miyoung Kim

Citation: Appl. Phys. Lett. **112**, 131901 (2018); doi: 10.1063/1.5018598
View online: https://doi.org/10.1063/1.5018598
View Table of Contents: http://aip.scitation.org/toc/apl/112/13
Published by the American Institute of Physics

Understanding luminescence properties of grain boundaries in GaN thin films and their atomistic origin

Hyobin Yoo,[1] Sangmoon Yoon,[1] Kunook Chung,[2] Seoung-Hun Kang,[3] Young-Kyun Kwon,[3] Gyu-Chul Yi,[2,a)] and Miyoung Kim[1,a)]
[1]*Department of Materials Science and Engineering, Seoul National University, Seoul 08826, Korea*
[2]*Department of Physics and Astronomy, Seoul National University, Seoul 08826, Korea*
[3]*Department of Physics and Research Institute for Basic Sciences, Kyung Hee University, Seoul 02447, Korea*

(Received 7 December 2017; accepted 12 March 2018; published online 26 March 2018)

We report our findings on the optical properties of grain boundaries in GaN films grown on graphene layers and discuss their atomistic origin. We combine electron backscatter diffraction with cathodoluminescence to directly correlate the structural defects with their optical properties, enabling the high-precision local luminescence measurement of the grain boundaries in GaN films. To further understand the atomistic origin of the luminescence properties, we carefully probed atomic core structures of the grain boundaries by exploiting aberration-corrected scanning transmission electron microscopy. The atomic core structures of grain boundaries show different ordering behaviors compared with those observed previously in threading dislocations. Energetics of the grain boundary core structures and their correlation with electronic structures were studied by first principles calculation. *Published by AIP Publishing*. https://doi.org/10.1063/1.5018598

GaN thin films have been extensively used to fabricate conventional optoelectronic devices such as light-emitting diodes and laser diodes. Despite the high density of threading dislocations formed in single crystalline GaN films, highly efficient and stable device operation was possible due to the fluctuation of energy gap in the optically active layer which segregates carriers away from the dislocations.[1–3] However, a more recent approach to integrate GaN into unconventional substrates such as van der Waals layered crystals, metals, and amorphous substrates for better functionalities has attracted great attention to polycrystalline GaN films, which entails additional microstructural defects such as grain boundaries.[4–18] Due to the extended form in two dimension, the grain boundaries are expected to play more significant roles in determining device performance compared with the dislocations. Thus, understanding the optical properties of the grain boundaries and their atomistic origin is crucial to engineer the optoelectronic building blocks in next-generation device applications.

The luminescence properties of microstructural defects such as threading dislocations in GaN films have long been controversial mainly because of the difficulties in spatially resolving the defects to correlate with their physical properties.[19–22] Moreover, limited information on atomic structures of the defects at the early stage of the related studies hindered reliable theoretical investigations on atomic and electronic origins.[23–27] Here, we combine electron backscatter diffraction (EBSD) and cathodoluminescence (CL) to directly correlate the structures of the grain boundaries and their luminescence properties. Furthermore, transferability of GaN films provided by layered structures of van der Waals crystals used as functional substrates facilitates the high quality electron microscopy sampling process for atomic scale structural analysis.[4,28] By exploiting aberration corrected scanning transmission electron microscopy (STEM) and density functional theory (DFT) calculation, we investigate the core structures of the grain boundaries at the atomic level and their corresponding electronic structures, respectively.

A GaN thin film was grown on chemically vapor deposited (CVD) graphene. The thin film consists of a high-temperature grown GaN layer (2.4 μm)/low-temperature grown GaN buffer layer (400 nm)/intermediate layer of ZnO nanostructures (160 nm)/graphene substrate.[4,5,9,10] EBSD and CL analyses were performed using a scanning electron microscope (SEM). The acceleration voltage was set to be 15 kV for EBSD and 5 kV for CL measurement. Plan-view TEM specimens were prepared by exfoliating the GaN films grown on CVD graphene from the arbitrary supporting substrates and further thinned by ion milling. Aberration corrected STEM operating at 200 kV was used for high-angle annular dark field (HAADF) STEM imaging with the probe convergence angle of 22 mrad and an inner collection semi-angle of 89.6 mrad. Noises arising in the HAADF STEM images were reduced by band pass filtering. The first principles calculation was carried out using the Vienna Ab initio Simulation Package pseudopotential code.

First, we examined the luminescence properties of the grain boundaries in GaN films by EBSD and CL. The combination of these two analytical methods allows direct correlation of the grain boundaries with their luminescence properties. As schematically represented in Fig. 1(a), positions of grain boundaries were located by the EBSD measurement, and CL analysis was conducted in the same region subsequently.

Figure 1(b) shows an SEM image that shows the morphology of the GaN thin film where we conducted EBSD and CL measurements. The GaN films grown on CVD graphene exhibited a flat surface morphology overall although they have a few pits and height variations, consistent with previous reports.[5,10,17] Figures 1(c) and 1(d) indicate the corresponding EBSD inverse pole figure (IPF) maps in the normal direction (ND) and rolling direction (RD), respectively.

a)Electronic mail: gcyi@snu.ac.kr, mkim@snu.ac.kr

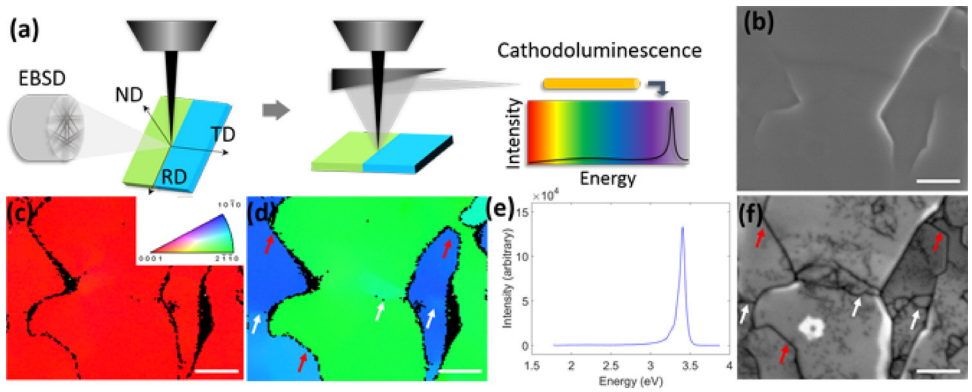

FIG. 1. Optical characterization of grain boundaries in the GaN thin films grown on CVD graphene. (a) Schematic representation of the measurement method for probing the local luminescence properties of the grain boundaries by a combination of electron backscatter diffraction (EBSD) and cathodoluminescence (CL). (b) Scanning electron microscopy image of the GaN thin films where EBSD and CL measurements were conducted. EBSD inverse pole figure maps in (c) the normal direction and (d) the rolling direction. The room temperature CL (e) spectrum and (f) panchromatic image obtained from the same region where the EBSD measurements were conducted are shown. Red and white arrows in (d) and (f) indicate the positions of high-angle and low-angle grain boundaries (misorientation angle for a low angle grain boundary $<3°$), respectively. The scale bar is 2 μm.

ND indicates the out-of-plane direction of the films, while the RD and transverse direction (TD) indicate two different in-plane directions of the films; all three directions are perpendicular to each other as represented in Fig. 1(a). The colors represented in ND and RD IPF maps indicate the crystallographic orientation with regard to the ND and RD of the films, respectively. Thus, the red color represented in the whole area of the ND IPF map indicates that the GaN thin films have a preferred orientation along the c-axis of the wurtzite structure in the out-of-plane direction (ND) of the films. In the meanwhile, in the rolling direction which is one of the in-plane directions, different colors were shown across the boundary which is displayed as black pixels where the backscatter diffraction could not be indexed to a desired accuracy. Hence, the black boundary across which green and blue colors were separated can be understood as high-angle tilt grain boundaries that are originated from the grain boundaries in CVD graphene due to the epitaxial relationship between GaN films and CVD graphene.[9] In this way, we could readily locate the position of the grain boundaries and obtain the information on the misorientation angles of those boundaries.

Subsequently, the CL measurement was performed for the correlation of defect structures and their corresponding luminescence properties. Figure 1(e) shows the room temperature CL spectrum which exhibits predominant near band edge emission at 3.4 eV. Yellow-band emissions that are reported to be observed when impurities or point defects are incorporated were not observed within the instrumental detection limit, indicating the high optical quality of the GaN films grown on the CVD graphene.

In order to investigate the spatial variation of the luminescence intensity of the near band edge emission along with the defect positions, we obtained a room temperature CL panchromatic image as shown in Fig. 1(f). The CL panchromatic image, an emission intensity map throughout the whole energy regime of the panchromatic detecting condition (1.5 eV–4.1 eV), can be understood as a spatial map of near band edge emission intensity which is the predominant emission in the spectrum. As shown in Fig. 1(f), dark regions were observed in the form of point-like features or linear features. The dark point-like features are presumably attributed to the presence of threading dislocations in the GaN films, which was previously reported.[21,22] Here, we note that the positions of grain boundaries that we verified earlier in the EBSD measurement were always coincident with linear dark regions observed in the CL panchromatic image. (Representative locations of those high-angle grain boundaries are indicated by red arrows in Figs. 1(d) and 1(f). This suggests that the intensity of the near band edge emission is suppressed at the high-angle grain boundaries in the GaN films. The reduced near band edge emission can be associated with either non-radiative recombination at the grain boundaries or radiative recombination with the emission energy less than 1.5 eV which is the instrument detection limit.

There are other locations in the films that also show linear dark contrasts in the CL panchromatic image such as the one we indicated with white arrows in Figs. 1(d) and 1(f). The structural element corresponding to the regions indicated with the white arrows is the low-angle grain boundary, which is verified by slight color difference across the boundaries in the RD IPF map in Fig. 1(d). Reduced near band edge emission in the low angle grain boundaries is consistent with the previous reports and showed a similar behavior to that of high-angle grain boundaries in the CL panchromatic image.[20]

We investigated the atomic structures of the high-angle grain boundaries to further understand the origin of the reduced near band edge emission at those locations. Here, we exploited aberration corrected STEM which offers an electron probe of sub-Ångstrom scale. The atomic configurations of the grain boundaries identified by the HAADF STEM technique were then used as initial models for DFT calculations to investigate the corresponding electronic density of states (DOS).

High resolution STEM analysis revealed that the high-angle grain boundaries were composed of arrays of a few types of dislocation core structures, with different arrangements depending on the misorientation angles between adjacent grains. The grain boundary shown in Fig. 2(a) exhibits a non-periodic array of different types of core structures, and they include all the representative types of core structures that we observed in the high-angle grain boundaries in the GaN

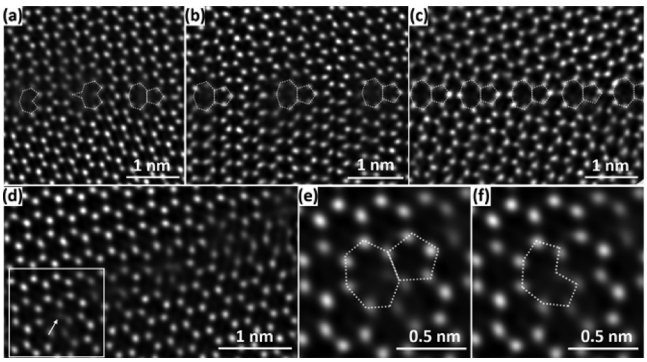

FIG. 2. Atomic resolution high-angle annular dark field (HAADF) scanning transmission electron microscopy (STEM) images of high-angle grain boundaries in the GaN thin films obtained from (a) the non-periodic boundary composed of different types of dislocation cores and coincident site lattice boundaries of (b) $\Sigma = 19$ and (c) $\Sigma = 7$ configurations. (d) HAADF STEM images taken from the $\Sigma = 7$ boundary that shows that one of the constituting dislocation cores has an atomic column with lower intensity as indicated by a white arrow. Enlarged images of the white squared region in (d) which are marked with (e) open-core and (f) full-core configurations are shown. Noises arising in the HAADF STEM images were reduced by band pass filtering.

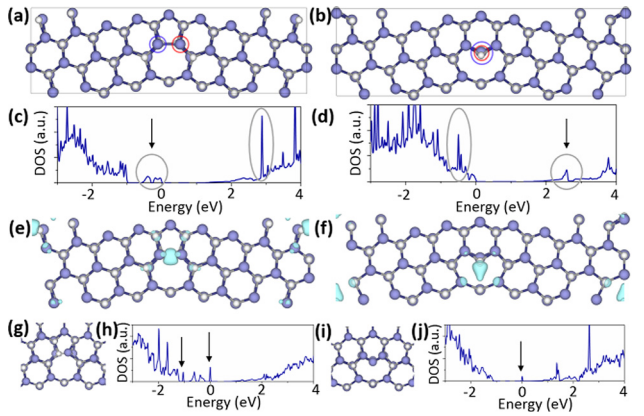

FIG. 3. (a) and (b) Structural models for the $\Sigma = 7$ boundary composed of (a) open-core structures and (b) full-core structures. (c) and (d) The density of states obtained from (c) open-core and (d) full-core boundaries. (e) and (f) Partial charge density projected on grain boundary structural models for (e) open-core and (f) full-core boundaries. (g) Relaxed core structure of the open-core boundary after forming Ga vacancy and (h) its corresponding density of states (DOS). (i) Relaxed core structure of the full-core boundary after forming N vacancy and (j) its corresponding DOS.

films. Three types of dislocation cores were observed; as indicated with white dashed lines in Fig. 2(a), 8-atom ring, 10-atom ring, and a pair of 7-atom and 5-atom rings constitute high-angle grain boundaries. Here, the 8-atom ring and the pair of 7-atom and 5-atom rings show similar configurations to full-core and open-core structures; the core structure configurations were first proposed on the edge-type threading dislocations in GaN films in early theoretical studies.[24,27] Here, we also use the same terminologies for the two core structures. In addition to the full- and open-core structures, the 10-atom ring shaped core structures were occasionally observed in the high-angle grain boundaries, which was not reported before. The three types of distinctive grain boundary cores all have the same Burgers vector of $\mathrm{b} = \frac{1}{3}\langle 2\bar{1}\bar{1}0\rangle$. Those cores were arranged in an irregular manner, in a way to accommodate lattice mismatch arising at the interface of the adjacent grains having a crystallographic misorientation.

We also observed periodically arranged high-angle grain boundaries as shown in Figs. 2(b) and 2(c). Mostly, open-core structures are arranged regularly with a fixed interval, forming coincident site lattice (CSL) twin boundaries; here, the grain boundaries shown in Figs. 2(b) and 2(c) are the $\Sigma = 19$ boundary and $\Sigma = 7$ boundary, respectively. As the misorientation angle of the grain boundaries increases, the dislocation cores need to be arranged more densely to accommodate the crystallographic misorientation. The intervals between the individual open cores are 0.74 nm for the $\Sigma = 19$ boundary with a 13° misorientation angle and 0.18 nm for the $\Sigma = 7$ boundary of 22°.

Here, we note that the open-core structure was the predominant core structure that constitutes high-angle grain boundaries, whereas the threading dislocations were mostly composed of full-core structures. Although there were theoretical predictions on both full-core and open-core structures at the edge-type threading dislocations,[23–27,29–32] the experimental evidence for the presence of open-core structures in the threading dislocations was based on conventional HR TEM imaging which could only offer indirectly interpretable images and require additional simulation for the atomic configuration determination. The phase problems arising from coherent nature of conventional HR TEM imaging and resolution limitation in association with lens aberration at the early stage made it less accurate to reconstruct the atomic arrangements.[30–33] In contrast, other previous experimental observations of the threading dislocations via directly interpretable incoherent imaging technique such as annular dark field STEM reported that all the edge-type threading dislocations showed full-core structures.[29,34–36]

We first examined the structural difference between the cores of the threading dislocations and the grain boundaries by DFT calculations. We made structural models for edge-type threading dislocations and grain boundaries which are composed of open-core and full-core structures, respectively [Figs. S2(a), S2(b), 3(a) and 3(b)]. Formation energies of dislocations and grain boundaries composed of open- and full-core structures were calculated and compared with each other (Table I). In the case of edge-type threading dislocations, the formation energy for the open-core structure is higher than that of the full-core structure by 1.7 eV/c, which is consistent with the previous theoretical studies and the experimental reports where they only observed full-core structures in the threading dislocations.[24,29,34,36] On the other hand, grain boundaries in GaN have rarely been studied theoretically. For representative case analysis, we chose the $\Sigma = 7$ boundary which is one of the most frequently observed boundary structures in the GaN films grown on CVD graphene. We calculated the formation energies of $\Sigma = 7$ boundaries composed of open-core structures and the one where we replaced the open-core structures with the full-core structures. The

TABLE I. Formation energy of full-core and open-core structures calculated for the threading dislocation and grain boundary, respectively.

	Full-core (eV/c)	Open-core (eV/c)
Dislocation	8.63	10.33
Grain boundary	5.71	5.33

formation energy of the open-core boundary was slightly lower than the full-core boundary by 0.38 eV, which is the opposite result compared with the threading dislocations. Accordingly, we could also verify by a theoretical approach that the open-core structures, which are energetically less favorable in the threading dislocations, can be prevalent core structures in the grain boundaries.

Although the atomic configuration of the grain boundaries composed of open-core structures was also predicted by indirect experimental evidence on unintentionally obtained grain boundaries and simulation analyses based on empirical potential calculations, their effect on the electronic structures have not been studied.[32,37,38] To further investigate the local luminescence characteristics of the grain boundaries, we investigated the electronic structures of the $\Sigma = 7$ boundaries by DFT calculation. For constructing the initial structural models, we note the following structural characteristics in the grain boundary cores. Although the open-core structure was predominantly observed in the grain boundaries, we sometimes observe the core structure which is difficult to be classified into either open- or full-core structures due to the lower intensity atomic column at the center [see the white arrow in Fig. 2(d)]. As shown in magnified images [Figs. 2(e) and 2(f)] of the white boxed region in Fig. 2(d), the dislocation core can be classified into open- or full-core structures depending on whether we count the atomic column with weak intensity as a full column (intensities of each atomic column were estimated from the unfiltered raw data in Fig. S7). Since the HAADF STEM images exhibit Z contrast intensity, the atomic column with lower intensity might have a less number of atoms along the beam direction, i.e., the atomic column may not be fully occupied. The partially occupied atomic column may be formed because of the compressive stress field, generated by the relatively shorter interatomic distances near the grain boundaries compared to those in bulk. Therefore, to understand the electronic structures of the grain boundaries more comprehensively, both open- and full-core boundary structures should be considered together despite much higher population of the open-core structures in the grain boundaries.

Accordingly, we construct the two atomic structure models for the $\Sigma = 7$ boundary as shown in Figs. 3(a) and 3(b). Figures 3(c) and 3(d) show the total DOS that were obtained for the stoichiometric grain boundaries shown in Figs. 3(a) and 3(b) after structural relaxation. Compared with the DOS of the bulk counterpart (Fig. S1), the DOS in the grain boundary structures showed additional localized states. As indicated with grey circles shown in Fig. 3(c), the stoichiometric grain boundary composed of open-core structures exhibited localized states within the bandgap and above the conduction band. In the case of the grain boundary composed of full-core structures, additional localized states were formed just above the conduction band minimum and under the valance band maximum.

To verify the origin of the localized states in the total DOS, we obtained the partial charge density projected on the relaxed grain boundary structures. Figures 3(e) and 3(f) show partial charge densities for the states that are marked with black arrows in Figs. 3(c) and 3(d), respectively. In both open- and full-core structures, the charge densities corresponding to the localized states were mostly concentrated in the core region of the grain boundaries, confirming the relationship between the localized defect states and the grain boundaries. Thus, the mid-gap states arising from open-core structures in the stoichiometric high-angle grain boundaries can be electrically active, reducing the near band edge emission intensity by impeding direct electronic transition from the conduction to the valence band.

We also studied the case where the grain boundaries become non-stoichiometric and further investigated how it affects the electronic structures. It was previously reported that the point defects in GaN films such as Ga or N vacancy often form and accumulate around the threading dislocations, making the dislocation non-stoichiometric. The resulting defect complex of the threading dislocations and the vacancies is believed to play a significant role in determining the optical behavior.[23,27,39] To understand how those point defects interact with the grain boundaries and change the electronic structures, we performed total energy calculations. The energetically favorable position to form those vacancies at the grain boundaries was indicated with blue circles shown in Figs. 3(a) and 3(b). We note that additional localized states were often formed in total DOS due to the presence of the point defects at the grain boundaries. For example, Fig. 3(g) shows a relaxed structure of the open-core $\Sigma = 7$ boundary having single Ga vacancy, and Fig. 3(h) shows the corresponding DOS which reveals additional mid-gap states as marked by arrows. Similarly, Fig. 3(i) shows a relaxed structure of the full-core boundary having a N vacancy in the energetically favorable position, and Fig. 3(j) shows the corresponding DOS. Although the stoichiometric grain boundary composed of full-cores exhibited no mid-gap states, the non-stoichiometric grain boundary with a N vacancy produced mid-gap states as marked with an arrow in Fig. 3(j).

Moreover, we carried out additional calculations for a higher concentration of vacancies. Given the single Ga or N vacancy formed in the blue circled region marked in Fig. 3(a), we confirmed that the additional Ga or N vacancy also prefers to form in the core region of the grain boundaries [red circles shown in Figs. 3(a) and 3(b)]. This indicates the strong possibility of point defect accumulation in the core region, and it is possibly associated with the partially occupied atomic columns that we investigated with the unfiltered HAADF STEM images shown in Fig. S6. The stress field localized on the grain boundary can act as traps for those point defects which is similar with the previous reports on the threading dislocation.[23] However, the detailed stress distribution around the grain boundary core is different from that of the dislocations, which is associated with the fact that the open-core structures are more stable configurations in grain boundaries.[40] Here, the corresponding DOS of the grain boundaries with accumulated point defects also show additional mid-gap states compared with those obtained for the grain boundary structure with single Ga or N vacancy. More detailed calculation results are discussed in the supplementary material.

According to the DFT calculation, the high-angle grain boundary structures and point defect accumulation produce multiple mid-gap states within the bandgap, and they can be the key factors to understand the reduced near band edge

emission at the grain boundaries. Electronic transition through those mid-gap states can be non-radiative since phonon generation becomes more favorable as the emission energy becomes smaller, but it can also be radiative with undesirable emission energy smaller than the instrument detection limit of the CL measurement. Although the mid-gap states might be formed in a different way depending on the misorientation angles, the overall tendency of forming mid-gap states in the grain boundary structure and their variations with the vacancy accumulation are expected generally in most of the high-angle grain boundaries.

In summary, the electron microscopy based study on the grain boundaries in GaN films combined with the DFT calculation provides useful insights into understanding the optical properties of the grain boundaries and their atomistic origin. The combination of EBSD and CL measurements directly reveals the local luminescence properties of the high-angle grain boundaries in GaN films. With the atomic resolution HAADF STEM, we confirmed that the high-angle grain boundaries were composed of arrays of various core structures with the open-core structure as the most prevalent type, which was different from the threading dislocations. Based on the atomic configurations observed by STEM analysis, we examined the corresponding electronic structure of the grain boundaries by DFT calculations. We believe that the mid-gap states formed by high-angle grain boundary structures and their variations with the accumulation of point defects are associated with the reduced near band edge emission at the high-angle grain boundaries.

See supplementary material for more details on the DFT calculation results and STEM analysis.

This research was supported by the National Research Foundation of Korea Grant (Nos. NRF-2017R1A2B3011629 and NRF-2015R1A5A1037627) and the TJ Park Science Fellowship of POSCO TJ Park Foundation.

[1]S. Chichibu, T. Azuhata, T. Sota, and S. Nakamura, Appl. Phys. Lett. **69**, 4188 (1996).
[2]Y. Narukawa, Y. Kawakami, M. Funato, S. Fujita, S. Fujita, and S. Nakamura, Appl. Phys. Lett. **70**, 981 (1997).
[3]S. Chichibu, K. Wada, and S. Nakamura, Appl. Phys. Lett. **71**, 2346 (1997).
[4]K. Chung, C.-H. Lee, and G.-C. Yi, Science **330**, 655 (2010).
[5]K. Chung, S. I. Park, H. Baek, J. S. Chung, and G.-C. Yi, NPG Asia Mater. **4**, e24 (2012).
[6]Y. Kobayashi, K. Kumakura, T. Akasaka, and T. Makimoto, Nature **484**, 223 (2012).
[7]C.-H. Lee, Y.-J. Kim, Y. J. Hong, S.-R. Jeon, S. Bae, B. H. Hong, and G.-C. Yi, Adv. Mater. **23**, 4614 (2011).
[8]J. M. Lee, J. W. Choung, J. Yi, D. H. Lee, M. Samal, D. K. Yi, C.-H. Lee, G.-C. Yi, U. Paik, J. A. Rogers, and W. I. Park, Nano Lett. **10**, 2783 (2010).
[9]H. Yoo, K. Chung, Y. S. Choi, C. S. Kang, K. H. Oh, M. Kim, and G.-C. Yi, Adv. Mater. **24**, 515 (2012).
[10]H. Yoo, K. Chung, S. I. Park, M. Kim, and G.-C. Yi, Appl. Phys. Lett. **102**, 051908 (2013).
[11]H. Baek, C.-H. Lee, K. Chung, and G.-C. Yi, Nano Lett. **13**, 2782 (2013).
[12]N. Han, T. Viet Cuong, M. Han, B. Deul Ryu, S. Chandramohan, J. Bae Park, J. Hye Kang, Y.-J. Park, K. Bok Ko, H. Yun Kim, H. Kyu Kim, J. Hyoung Ryu, Y. S. Katharria, C.-J. Choi, and C.-H. Hong, Nat. Commun. **4**, 1452 (2013).
[13]A. Yamada, K. P. Ho, T. Akaogi, T. Maruyama, and K. Akimoto, J. Cryst. Growth **201**, 332 (1999).
[14]A. Yamada, K. P. Ho, T. Maruyama, and K. Akimoto, Appl. Phys. A-Mater. Sci. Process. **69**, 89 (1999).
[15]J. Liao, B. Sa, J. Zhou, R. Ahuja, and Z. Sun, J. Phys. Chem. C **118**, 17594 (2014).
[16]H. Zhang, Y.-N. Zhang, H. Liu, and L.-M. Liu, J. Mater. Chem. A **2**, 15389 (2014).
[17]K. Chung, H. Yoo, J. K. Hyun, H. Oh, Y. Tchoe, K. Lee, H. Baek, M. Kim, and G. C. Yi, Adv. Mater. **28**, 7688 (2016).
[18]Y. Zhang, X. Li, L. Wang, X. Yi, D. Wu, H. Zhu, and G. Wang, Nanoscale **4**, 5852 (2012).
[19]S. D. Lester, F. A. Ponce, M. G. Craford, and D. A. Steigerwald, Appl. Phys. Lett. **66**, 1249 (1995).
[20]F. A. Ponce, D. P. Bour, W. Gotz, and P. J. Wright, Appl. Phys. Lett. **68**, 57 (1996).
[21]S. J. Rosner, E. C. Carr, M. J. Ludowise, G. Girolami, and H. I. Erikson, Appl. Phys. Lett. **70**, 420 (1997).
[22]T. Sugahara, H. Sato, M. Hao, Y. Naoi, S. Kurai, S. Tottori, K. Yamashita, K. Nishino, L. Romano, and S. Sakai, Jpn. J. Appl. Phys., Part 2 **37**, L398 (1998).
[23]J. Elsner, R. Jones, M. I. Heggie, P. K. Sitch, M. Haugk, T. Frauenheim, S. Öberg, and P. R. Briddon, Phys. Rev. B **58**, 12571 (1998).
[24]J. Elsner, R. Jones, P. Sitch, V. Porezag, M. Elstner, T. Frauenheim, M. Heggie, S. Öberg, and P. Briddon, Phys. Rev. Lett. **79**, 3672 (1997).
[25]S. M. Lee, M. A. Belkhir, X. Y. Zhu, Y. H. Lee, Y. G. Hwang, and T. Frauenheim, Phys. Rev. B **61**, 16033 (2000).
[26]K. Leung, A. F. Wright, and E. B. Stechel, Appl. Phys. Lett. **74**, 2495 (1999).
[27]A. F. Wright and U. Grossner, Appl. Phys. Lett. **73**, 2751 (1998).
[28]J. Jo, H. Yoo, S.-I. Park, J. B. Park, S. Yoon, M. Kim, and G.-C. Yi, Adv. Mater. **26**, 2011 (2014).
[29]Y. Xin, S. J. Pennycook, N. D. Browning, P. D. Nellist, S. Sivananthan, F. Omnes, B. Beaumont, J. P. Faurie, and P. Gibart, Appl. Phys. Lett. **72**, 2680 (1998).
[30]P. Ruterana, V. Potin, G. Nouet, R. Bonnet, and M. Loubradou, Mater. Sci. Eng. B-Solid State Mater. **59**, 177 (1999).
[31]A. Béré and A. Serra, Phys. Rev. B **65**, 205323 (2002).
[32]V. Potin, P. Ruterana, G. Nouet, R. Pond, and H. Morkoç, Phys. Rev. B **61**, 5587 (2000).
[33]A. Bourret, J. Rouviere, and J. Penisson, Acta Crystallogr. Sect. A **44**, 838 (1988).
[34]Y. Xin, E. James, I. Arslan, S. Sivananthan, N. Browning, S. Pennycook, F. Omnes, B. Beaumont, J. Faurie, and P. Gibart, Appl. Phys. Lett. **76**, 466 (2000).
[35]P. Nellist and S. Pennycook, Ultramicroscopy **78**, 111 (1999).
[36]I. Arslan, A. Bleloch, E. A. Stach, and N. D. Browning, Phys. Rev. Lett. **94**, 025504 (2005).
[37]A. Bere and A. Serra, Philos. Mag. **86**, 2159 (2006).
[38]J. Chen, P. Ruterana, and G. Nouet, Phys. Status Solidi A-Appl. Mater. **203**, 247 (2006).
[39]J. Neugebauer and C. G. Van de Walle, Appl. Phys. Lett. **69**, 503 (1996).
[40]S. Yoon, H. Yoo, S.-H. Kang, M. Kim, and Y.-K. Kwon, Sci. Rep. **8**, 4647 (2018).